Iranian Journal of Science and Technology, Transactions of Civil Engineering (2024) 48:3173–3187
https://doi.org/10.1007/s40996-023-01341-1

RESEARCH PAPER

A Comprehensive Study on Optimizing Activator Composition for Enhanced Strength and Micro-Structure in High-Strength Alkali-Activated Slag Binders

Shivam Kumar[1] · **Pramod Kumar Gupta**[1] · **Mohd. Ashraf Iqbal**[1]

Received: 14 September 2023 / Accepted: 22 December 2023 / Published online: 23 January 2024

Abstract
The production of Portland cement involves exploiting natural reserves of limestone and coal and emitting approximately one metric tonne of carbon dioxide for every metric tonne of cement produced. This article investigates the optimisation of alkaline activators for enhanced strength and micro-structure in high-strength alkali-activated slag binders/mortars to explore alternative construction materials that are environmentally sustainable, require less energy consumption, and offer greater cost-effectiveness. The study reveals that the AAS binder and cement exhibit comparable hydration characteristics. However, the AAS binder demonstrates a shorter dormancy period, an earlier and heightened second exothermic peak, lower cumulative heat and inadequate $Ca(OH)_2$ crystallisation. Furthermore, the AAS binder has a lower Ca/Si ratio and a higher Al/Si ratio in the gels. The pore structure of hardened AAS binder consistently shows higher compressive strength and denser, more stable micro-structure than cement paste, particularly in the early stages. Alkali-activated slag (AAS) mortar exhibits a 52–89% increase in compressive strength compared to cement mortar, suggesting the potential of AAS binder to replace cement. The compressive strength of AASM-4 mortar mix with a Na_2O concentration of 7%, an activation modulus of 1.2, and a water-to-binder ratio of 0.4 is 89.4 MPa after 28 days of air curing. Furthermore, all mortar mixes featuring Na_2O concentrations between 4 and 7% achieved over 70% of their 28-day compressive strength within seven days. In conclusion, the research posits that the AAS binder has the potential to replace cement as a building material in specific engineering applications, mainly when high strength is a requirement.

Keywords Alkali-activated slag paste · Cement paste · Mortar · Micro-structural analysis · Compressive strength · Heat of hydration

1 Introduction

The increasing emission of greenhouse gases, particularly carbon dioxide, has generated global concerns over climate change. Concrete, an extensively utilised material in the construction industry, necessitates significant quantities of Portland cement—this dependency on Portland cement results in exploiting limestone and coal's natural reserves. Cement production emits about one metric tonne of carbon dioxide for every metric tonne of cement produced, resulting in environmental strain. Worldwide, the cement industry contributes around 5–7% of the total atmospheric carbon dioxide (CO_2) emissions (Kumar et al. 2023a). Therefore, it is necessary to develop alternative construction materials that are ecologically sustainable, exhibit enhanced durability, demand less energy consumption, and offer more cost-effectiveness. The increasing growth of the iron and steel industry has led to the generation of substantial quantities of granulated blast furnace slag (GBFS), which poses environmental difficulties regarding waste disposal. Disposal of industrial waste has grown difficult and costly because of the progressively strong environmental laws and regulations and the scarcity of suitable dumping grounds nearby. These environmental considerations have motivated researchers to explore innovative binding materials that replace ordinary Portland cement (OPC) with AASB, fly ash and rice husk ash (Mareya et al. 2023; Sithole et al. 2021a). AASB is a relatively new cementitious material that has gained popularity

✉ Shivam Kumar
skumar18@ce.iitr.ac.in

[1] Department of Civil Engineering, Indian Institute of Technology Roorkee, Roorkee 247667, India

due to its potential to reduce CO_2 emissions, lower energy consumption, and improve sustainability in the construction industry. (Kumar et al. 2023b; Sithole et al. 2019, 2021b; Sithole and Mashifana 2020). It has the potential to significantly reduce carbon dioxide emissions by up to 70–80%, making it an environmentally friendly option (Provis 2018). In India, GGBS has an annual production of 15 million tons, with only 55% being utilized in the construction sector. Hence, it is crucial to enhance the application of industrial waste on a broader scale within the concrete industry to reap environmental advantages (Pandhare and Jayaraj 2023).

Alkali-activated slag (AAS) binders are typically produced by mixing ground granulated blast-furnace slag (GGBS) with an alkaline activator, such as sodium hydroxide (NaOH), potassium hydroxide (KOH), sodium silicate (SS), potassium silicate, or a mixture of these. It involves the reaction of the alkaline activator solution with the slag, which forms a gel-like material (Sithole et al. 2022). This gel-like material, such as C-A-S–H and a hydrotalcite-like phase, is responsible for the strength and durability of the AAS binder (Schade et al. 2022). The scientific use of GGBS in the production of AAMs involves understanding of chemical reactions that occur during the activation process and how these reactions affect the properties of the resulting material (Al Makhadmeh and Soliman 2020). The curing conditions (Bilim et al. 2015; Salman et al. 2015a), particle size and chemical composition of the slag (Humad et al. 2019) also impact the properties of the AAS binder. The use of GGBS in AAMs can improve the mechanical properties, durability, and resistance to acid and sulphate attack of the resulting material (Bingöl et al. 2020; Venkatesan and Pazhani 2016). However, the performance of AAMs can vary depending on the specific conditions and materials used. Further research is needed to deeply understand the potential of GGBS and alkaline activators in alkali-activated materials.

Studies have shown that the durability of an alkali-activated slag binder (AASB) is comparable to that of Portland cement. However, impurities in the slag can lead to the formation of deleterious phases, which can affect AASB's durability (Wang et al. 2020). The chemical composition of slag affects the reactivity of the material, promoting better reactivity and strength development with higher amounts of silica and alumina in slag (Zhang et al. 2022). Careful control of curing conditions is essential to ensure the durability of AASB, with higher temperatures and moist curing conditions promoting faster reaction rates and better strength development (Nasr et al. 2018). The type and amount of alkali activator used in AASB influence the rate of reaction, and excessive shrinkage and cracking can occur with higher concentrations (Navarro et al. 2022). AASB has better chloride resistance than ordinary Portland cement due to its lower porosity and higher density, inhibiting chloride ion penetration (Mangat et al. 2021). Due to the high level of C–A–S–H gel polymerization and fine porosity, which results in a relatively dense micro-structure and complex pore interconnection, alkali-activated slag demonstrated superior resistance to chloride transport (Runci et al. 2022). AAS has a benefit over other OPC alternatives since it attained a very low chloride diffusion coefficient just after 7 days, which is beneficial for its use in marine applications (Runci and Serdar 2022). The micro-structural behaviour of AASB is complex, influenced by several factors such as the composition and concentration of the activator solution, curing conditions, and chemical and mineralogical properties of the slag (Arioz et al. 2020; Navarro et al. 2022). AASB has a more heterogeneous micro-structure than OPC, with varying products depending on the slag and activator solution (Tushar et al. 2022). The use of AAS binder is still limited because of some challenges that remain in adopting AASB, such as the lack of standardized production protocols, limited commercial availability, and issues related to the long-term stability of the materials. Further research is needed to address these challenges and promote the adoption of AAS binder as a sustainable building material (Kar et al. 2014; Lanjewar et al. 2023).

AASB is a promising alternative to Portland cement with several significant aspects. As the demand for sustainable building materials increases, the development and adoption of AASB are likely to continue growing in the coming years. Although the research has been conducted on alkali-activated slag binders in recent years, there are still some gaps that require attention. Gaining insight into the reaction mechanism and products of alkali-activated slag remains an ongoing challenge, as the mechanism is not yet fully understood. Despite the use of various activators to activate slag, a systematic study on the optimization of the alkaline activator concentration is still lacking to produce high-strength AASB. Ongoing research aims to deepen our understanding of its micro-structural behaviour on physical properties and enhance its applications, including the development of new high-performance alkali-activated slag binders (AASB). The focus of the present study is the effects of different activator components and their concentrations on the properties of the alkali-activated slag binder/mortar. The calorimetric studies of hydration processes were performed to investigate the early stages behaviour of alkali-activated blast-furnace slag binder in comparison with OPC. Advanced techniques such as X-ray diffraction (XRD), field emission scanning electron microscopy (FE-SEM), thermogravimetry analysis (TGA), and energy-dispersive X-ray spectroscopy (EDX) were performed to deeply understand the reaction products of alkali-activated slag binders.

Table 1 The chemical properties of GGBS

Chemical Constituents	Na_2O	MgO	Al_2O_3	SiO_2	SO_3	Cl	K_2O	CaO	TiO_2	MnO	Fe_2O_3	Minor minerals
GGBS (% of weight)	0.19	5.05	18.17	33.56	1.22	0.01	0.51	38.91	0.71	0.99	0.54	0.14

2 Materials and Methodology

Alkali-activated slag binders were produced by the activation of GGBS with an alkaline solution. Alkaline solution was a mixture of sodium hydroxide pellets and sodium silicate liquid.

2.1 Material Characterization

The characterization of materials used in this study, such as GGBS and alkaline solution, is discussed in this section in terms of their chemical composition, particle size distribution, mineralogy, and reactivity.

2.1.1 Ground Granulated Blast-Furnace Slag (GGBS)

GGBS is a by-product of the steel-making process and is known to have cementitious and pozzolanic properties, which can react with calcium hydroxide in water to form a cementitious material. GGBS in AAMs offers several benefits, including reduced CO_2 emissions, lower production costs, and the ability to utilize a waste product in a useful application. The use of GGBS in the production of AAMs offers a promising alternative to traditional Portland cement-based materials, with potential benefits for both the environment and the economy. In this study, GGBS obtained from Jindal Steel Works, Bellary, India, was utilized as a binder to synthesize Alkali-activated slag binder. The GGBS had a specific gravity of approximately 2.91 and a specific surface area of 390 m^2/kg. The chemical properties of the GGBS were determined through X-ray fluorescence (XRF) analysis and are presented in Table 1.

The hydraulic activity of GGBS can be determined by computing its basicity coefficient (K_b). For the development of an alkali-activated cement, GGBS requires a minimum glass content of 70% and a basicity coefficient (K_b) falling between 0.7 and 1.2 (Shi et al. 2006), where

$$K_b = \frac{(\mathrm{CaO} + \mathrm{MgO})}{(\mathrm{SiO_2} + \mathrm{Al_2O_3})}$$

According to the basicity coefficient, GGBS can be classified into three categories: neutral ($K_b = 1$), alkaline ($K_b > 1$), and acidic ($K_b < 1$). Typically, alkaline and neutral slags are more desirable as binders. However, the GGBS utilized in this study contained 90% glass content (as supplied by the manufacturer) and had a basicity coefficient of 0.85, indicating an acidic nature. As a result, an alkaline solution was employed to adjust the pH to a neutral or alkaline level.

Table 2 Characteristics of sodium silicate liquid (SS)

Chemical formula	Na_2SiO_3
Specific gravity (SG_{SS})	1.57
Components	% by weight
Na_2O	14.5
SiO_2	32.9
Water Content	52.6

Table 3 Characteristic of sodium hydroxide pellets (97% purity)

Chemical formula	(NaOH)
Specific gravity (SG_{NaOH})	2.1
Physical appearance	White chips or flakes
Molecular mass	39.99 g per mole
Solvability (in water)	114/100 ml

2.1.2 Alkaline Activator Solution

An alkaline activator solution, a chemical solution containing a high pH (above 7), was used to activate GGBS and accelerate the setting and hardening of the AAS binders. The alkaline solution used in this paper contains a source of alkalinity, such as sodium hydroxide (NaOH), and a source of silica, such as sodium silicate (SS). The blended NaOH and SS solution was characterised by the activator modulus (Ms), where

$$\mathrm{M_S} = \frac{\mathrm{SiO_2}}{\mathrm{Na_2O}}$$

Varied M_s values were attained through the manipulation of the proportion of SS to NaOH in the alkaline solution. The alkaline activator solution was prepared 24 h in advance of its application. The alkaline activator solution triggers a chemical reaction between the binding material, such as GGBS and the activator solution, resulting in the formation of an AAS binder. Alkaline activator solutions are an area of active research in materials science and engineering, with ongoing efforts to optimize their composition and performance for various applications, including alkali-activated

slag binders. Tables 2 and 3 contain information on the properties of SS and NaOH, respectively, which were utilized in the preparation of an alkaline solution as described herein (Fig. 1).

2.2 Reaction Mechanism

The reaction mechanism of the AAS binder involves a complex series of chemical reactions between the GGBS and the alkaline activator solution. The reaction mechanism of an AAS binder involves several steps, such as dissolution, polymerization, condensation, and hardening. When the alkaline activator solution is mixed with GGBS, the alkali ions (e.g. Na^+) react with the silica (SiO_2) and alumina (Al_2O_3) components of the slag, causing the dissolution of the slag particles. This process involves the breaking of covalent bonds between silicon, aluminium and oxygen atoms by releasing cations such as calcium (Ca^{2+}) and magnesium (Mg^{2+}) ions. This process is exothermic and releases intense heat. Now, the dissolved GGBS contains silica and alumina components, which react with the alkaline solution to form polymeric species, such as sodium silicate and sodium aluminate, which act as precursors for the formation of the cementitious phases. These polymeric species undergo further condensation reactions, in which the silica and alumina molecules link up to form a three-dimensional network of bonds. This network is known as the geo-polymer matrix, which provides the strength and durability of the material (Cao et al. 2020; Los, n.d.).

2.3 Test Matrix and Specimens' Preparation

Table 4 presents the details of the key parameters and the designed mix proportions of all the samples. To prepare the AAS binder samples for the heat of hydration testing, sodium silicate (SS) and sodium hydroxide (NaOH) were pre-dissolved in water and then cooled to room temperature for 24 h before being mixed to GGBS (see Fig. 2a). In a plastic zip bag, GGBS was precisely measured (see Fig. 2b), and then the alkaline solution was gradually added and thoroughly mixed (see Fig. 2c). The rate of heat evolution and hydration heat release of a cement paste (CP) sample and eight AASB samples with a constant water/binder ratio of 0.4 was determined using I-Cal 4000 HPC, a 4-channel Isothermal high precision calorimeter manufactured by calmetrix as shown in Fig. 2e. The specimens that underwent the heat of hydration tests served as the source of all the collected samples used to investigate their micro-structural behaviour, which includes XRD, TGA, FE-SEM, and EDX. The broken specimen samples were ground in an agate mortar (as shown in Fig. 3a) and used for the testing of XRD and TGA, and the small pieces of broken samples, as shown in Fig. 3b, was used for FE-SEM and EDX tests. For XRD analysis, we utilized the Bruker D8 ADVANCE equipment with a long fine-focus ceramic X-ray tube containing a Cu

Fig. 1 Images of **a** GGBS, **b** sodium hydroxide pellets, and **c** sodium silicate liquid

Table 4 Details of parameters and designed proportions of alkali-activated slag binder

Sample ID	Key parameters				Cement 'or' GGBS (g)	SS (g)	NaOH (g)	water added externally (g)
	Binder type	w/b	Na_2O%	Ms				
CP	Cement	0.4	–	–	60	–	–	24
AASB-1	GGBS	0.4	4	1.2	60	8.75	1.46	19.40
AASB-2	GGBS	0.4	5	1.2	60	10.94	1.82	18.24
AASB-3	GGBS	0.4	6	1.2	60	13.13	2.19	17.09
AASB-4	GGBS	0.4	7	1.2	60	15.32	2.55	15.94
AASB-5	GGBS	0.4	4	1.0	60	7.29	1.73	20.16
AASB-6	GGBS	0.4	5	1.0	60	9.12	2.16	19.20
AASB-7	GGBS	0.4	6	1.0	60	10.94	2.60	18.24
AASB-8	GGBS	0.4	7	1.0	60	12.77	3.03	17.29

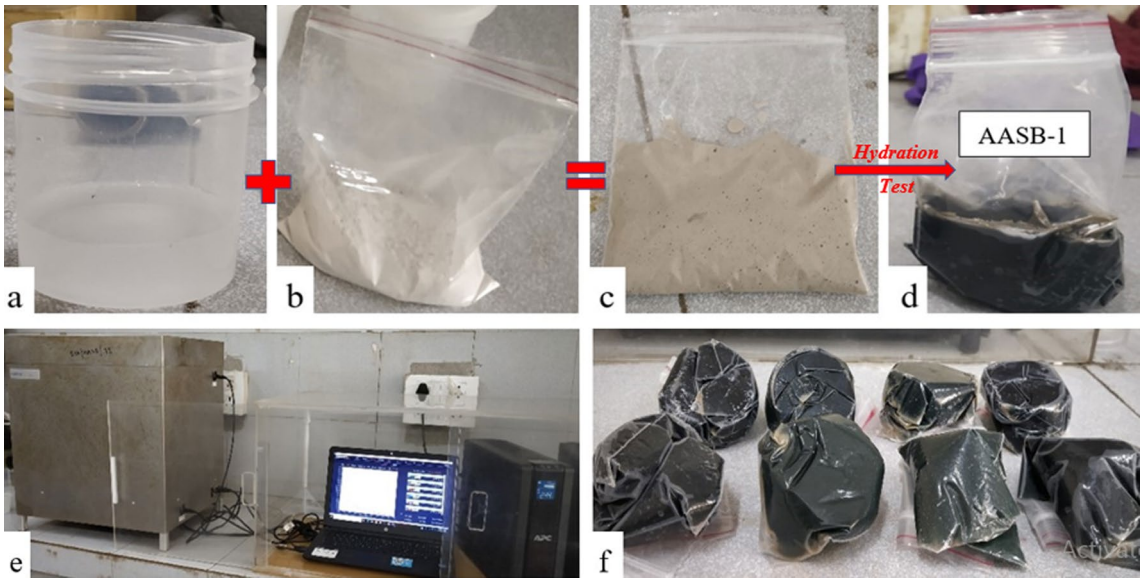

Fig. 2 Images of **a** alkaline solution, **b** GGBS in a plastic zip bag, **c** GGBS mixed with the alkaline solution, **d** AASB-1 sample after test, **e** I-Cal 4000 HP calorimeter, and **f** all AAS samples after hydration heat test

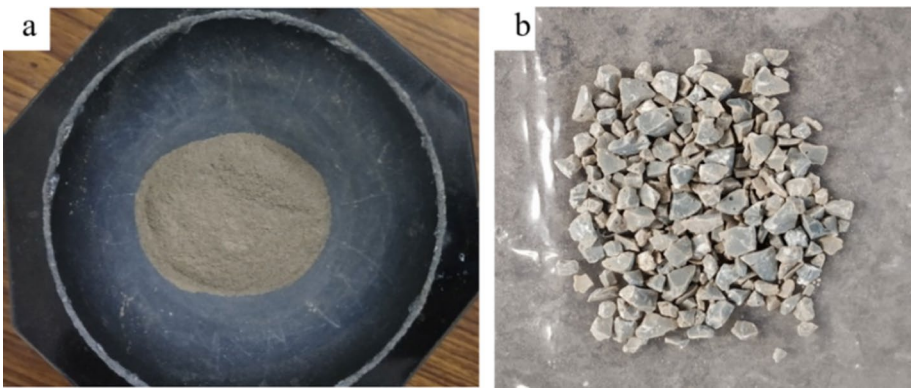

Fig. 3 Sample prepared for **a** XRD and TGA and **b** FE-SEM and EDX tests

anode, which operated at a voltage of 40 kV and a working current of 40 mA. The X-ray source had a power output of 2.2 kW. For TG analysis, we employed the SII 6300 EXSTAR device manufactured by Seiko Instruments Inc. to analyse the morphology of the hydrates. In addition, we used the Carl-Zeiss-Gemini scanning electron microscope for SEM and EDX analysis. This thermal-type field emission instrument had a stability better than 0.2%/h and a magnification range of 12–200,000X (SE) and 100–100,000X (BSE), with a resolution of up to 0.8 nm.

To investigate the compressive strength of the AAS binders mentioned in Table 4, alkali-activated slag mortar cubes were made in line with Indian Standard IS:4031(Part 6). The standard sand were used as per the Indian standard (IS 650:1991, 1991) and the binder-to-standard sand weight ratio was 1:3. The material was mixed separately for each cube. The alkaline solution was premixed before 24 h of its use. Mortar cubes were manufactured to determine compressive strength, with dimensions of 70.6 × 70.6 × 70.6 mm (IS: 4031 (Part 6), 2006). The compressive strength of the test specimens was evaluated at 1, 3, 7, and 28 days. The mortar cubes of alkali-activated slag binder were subjected to room temperature curing, and the cement cubes were submerged in the running water. The precise mix proportions for cement mortar (CM) and all the alkali-activated slag mortars (AASM) in this investigation are shown in Table 5.

3 Results and Discussion

3.1 Compressive Strength of Mortar Cubes

Figure 4 displays examined samples of cubes made from alkali-activated slag mortar (AASM), while Fig. 5 illustrates

Table 5 Details of designed proportions of alkali-activated slag mortar

Sample ID	Cement 'or' GGBS (g)	SS (g)	NaOH (g)	Extra water (g)	Standard sand for testing cement specification (g)		
					Grade-I	Grade-II	Grade-III
CP	200	–	–	80	200	200	200
AASM-1	200	32.7	4.1	61.7	200	200	200
AASM-2	200	40.8	5.2	57.2	200	200	200
AASM-3	200	49.0	6.2	52.6	200	200	200
AASM-4	200	57.1	7.2	48.1	200	200	200
AASM-5	200	27.2	5.2	64.8	200	200	200
AASM-6	200	34.0	6.5	61.0	200	200	200
AASM-7	200	40.8	7.7	57.2	200	200	200
AASM-8	200	47.6	9.0	53.4	200	200	200

g denotes the weight in grams

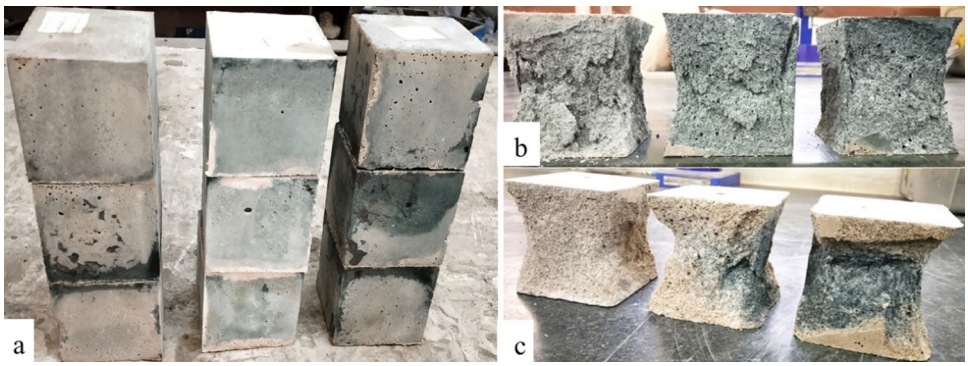

Fig. 4 Images of the AAS mortar cubes **a** before testing and testing at **b** 1 day, and **c** 28 days

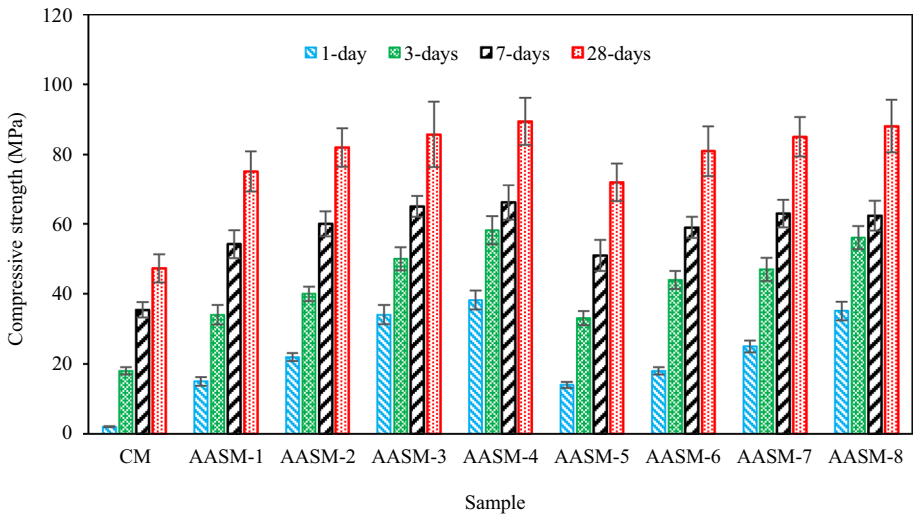

Fig. 5 Compressive strength of all the AASM samples at 1, 3, 7, and 28 days

the compressive strength outcomes for a control cement mortar (CM) and eight AASM samples. This investigation specifically explores the impact of Na_2O% and Ms (SiO_2/Na_2O) ratios on the development of compressive strength. It can be concluded that an increase in Na_2O% resulted in an increase in the compressive strength of the cubes. This effect is attributed to the higher concentration of OH- ions, which disrupted the Si–O bonds on the surface of slag particles, leading to the formation of a greater quantity of hydration products, particularly C–A–S–H gel. The observed increase in compressive strength was more significant for mixtures with higher Ms ratios, as escalating Ms values prompted the transformation of a loosely packed structure into a denser and more compact arrangement, thereby reducing porosity.

Higher Ms values also provided more reactive silica, which enhanced the geo-polymerization process, leading to the formation of a larger amount of C–A–S–H gel (Al Makhadmeh and Soliman 2020). The 28-day compressive strength increased as Na_2O concentration increased from 4 to 6% but increasing Na_2O% from 6 to 7% did not cause a significant improvement in strength. The optimum Ms ratio to achieve the highest 28-day compressive strength for basic slag was 1.2. Furthermore, an increase in Na_2O concentration from 4 to 7% led to an average increase of 19% and 22.4% in the 28-day compressive strength at Ms values of 1.2 and 1.0, respectively. The compressive strength values of AASM cubes were found to be greater than those of cement mortar, exhibiting a substantial increase of approximately 80–90% in strength.

3.2 Parametric Sensitivity Analysis

A parametric sensitivity analysis was conducted to develop a deep understanding of the effects of alkali-activators, such as Na_2O% and Ms value, on the compressive strength of AASB. Figure 6a–d illustrates the impact of key parameters, such as Na_2O% and Ms value, on the compressive strength of AASM. The origin of the axis indicates that any relative change in the parameters is linked to a relative change in the response, corresponding to the reference values of key parameters. The reference values for these parameters, taken from a mixture (i.e. AASM-6) in this study, are presented in Table 6. In these non-dimensional axes, "+" and "-" indicate an increase and decrease, respectively. The findings demonstrated that increasing Na_2O% from 4 to 7 and Ms value from 1 to 1.2 results in an increase in compressive strength. This means that compressive strengths are directly proportional to Na_2O% and Ms value. It can be observed from Fig. 6a-d that

Table 6 Reference values of key parameters selected for the mechanical response analysis

Parameter	w/b ratio	% of Na_2O	Ms value
Reference value	0.40	7	1.2

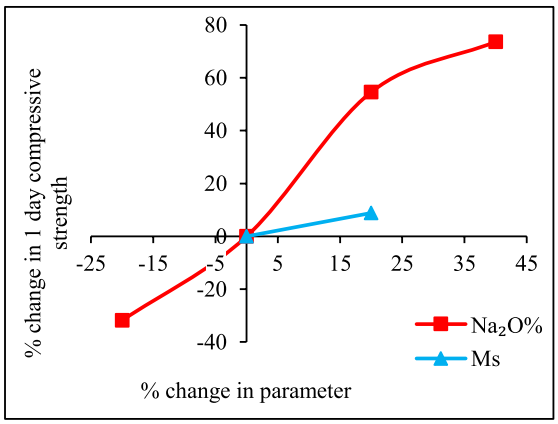

(a) Sensitivity of 1-day compressive strength

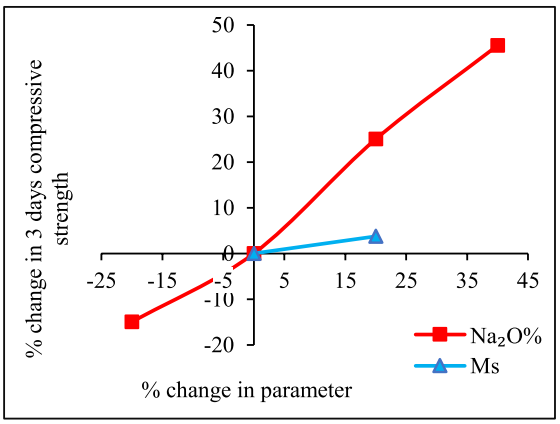

(b) Sensitivity of 3 days compressive strength

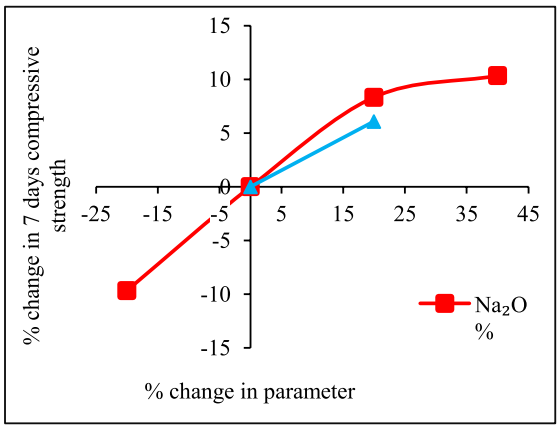

(c) Sensitivity of 7 days compressive strength

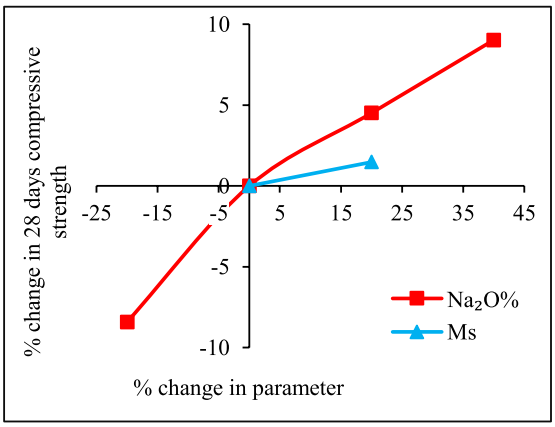

(d) Sensitivity of 28 days compressive strength

Fig. 6 Sensitivity of the compressive strengths of AASM samples

compressive strength is most sensitive to changes in Na_2O%, followed by the Ms value.

3.3 Heat of hydration

The process of hydration involves a series of events, including dissolution, induction, acceleration, deceleration, and ultimately achieving a state of steady-state diffusion. Previous research (Al Makhadmeh and Soliman 2022; Brough and Atkinson 2002) has extensively documented these stages. The pre-induction phase marks the rapid dissolution of ionic species that occurs upon immediate contact of cement with water and slag with the activator solution, resulting in the formation of the initial peak. This peak signifies the release of heat, intense in a short timeframe, attributed to swift hydration. Following this, the heat evolution curves decline, and the period during which the hydration progresses slowly is termed the induction period. The appearance of the second peak is associated with the development of primary hydration-induced products, namely calcium silicate hydrate and aluminate silicate hydrates (Usherov-marshak et al., 2021). The intensity of the second peak is relatively less pronounced than the first. In the post-acceleration phase, the hydration rate gradually slows, transitioning to diffusion control (Fig. 7).

In Fig. 8a, pastes are distinguished by varying proportions of Na_2O concentration with a constant activation modulus of 1.2. Conversely, in Fig. 8b, the distinction is based on varying proportions of Na_2O% with a constant activation modulus of 1.0. The experiments were carried out using a water-to-binder ratio of 0.4 at a constant temperature of 25 °C. Figure 7 shows the testing setup for heat of hydration tests. The study involved examining the heat evolution rate of nine samples, consisting of one control sample of cement paste and eight alkali-activated slag binder samples. In all these samples, the initial peak occurred within a time frame of 0.4 h, while the second peak was observed between 8.0 and 15.0 h after the start of the reaction, which corresponded to the formation of reaction products. Notable differences were observed in the magnitudes of these peaks. The second hydration peak in the alkali-activated slag binder with 7% of Na_2O exceeded that of binders with 4%, 5%, or 6% of Na_2O, as well as surpassing the peak observed in cement paste. Increasing the percentage of Na_2O led to earlier and higher hydration peaks, along with the shorter induction periods. All curves exhibited a substantial induction period ranging from about 2 to 6 h before the second peak. It can be concluded that increasing Na_2O dosage inversely correlates with the induction period.

3.3.1 Cumulative Heat of Hydration

In Fig. 9, the cumulative heat of hydration is illustrated for CP and AASBs. It is noted that an increase in the cumulative heat of hydration occurs when both the dosage of slag and the concentration of sodium oxide (Na_2O) are increased. This suggests that higher amounts of GGBS and Na_2O result in a more pronounced heat release during the hydration process. However, there is an interesting observation regarding the activation modulus. Increasing the activation modulus has a negative impact on the cumulative heat of hydration, as depicted in Fig. 10. The activation modulus is a parameter that influences the reactivity of the alkali activator in AASBs.

During the first 24 h, alkali-activated slag pastes with different activation modulus and percentages of Na_2O release higher heat than cement paste (CP) at a given isothermal temperature for all activator dosages. However, after 24 h, alkali-activated slag pastes release less heat than cement paste at a given isothermal temperature for all activator dosages. This implies that, in the initial stages, AASBs exhibit higher heat of hydration, and after 24 h, the heat of hydration slows down compared to traditional cement paste. In conclusion, the heat of hydration contribution for alkali-activated slag binders is dependent on various factors. These factors include the nature of the GGBS used, as well as the activation modulus and percentage of Na_2O employed in the mixture. This underscores the complexity of the hydration

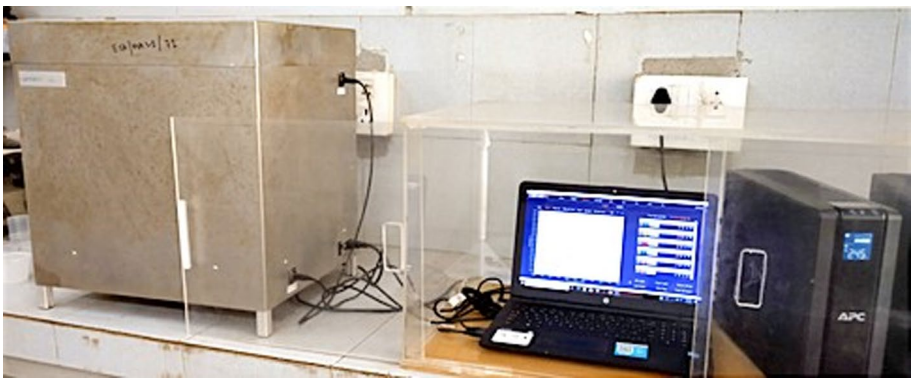

Fig. 7 Testing setup for heat of hydration tests

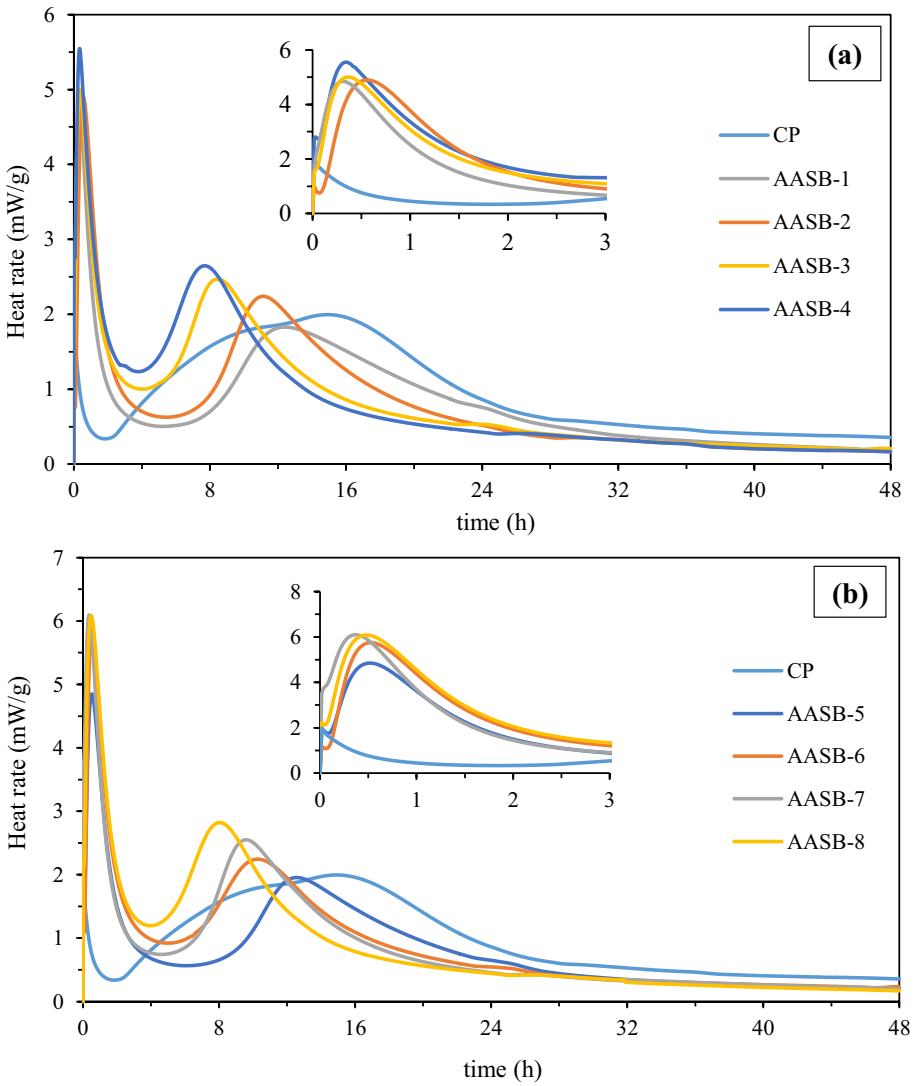

Fig. 8 Hydration heat rate of a cement paste (CP) and various AASB samples with varying concentrations of Na_2O and activation modulus of **a** Ms = 1.2 and **b** Ms = 1.0

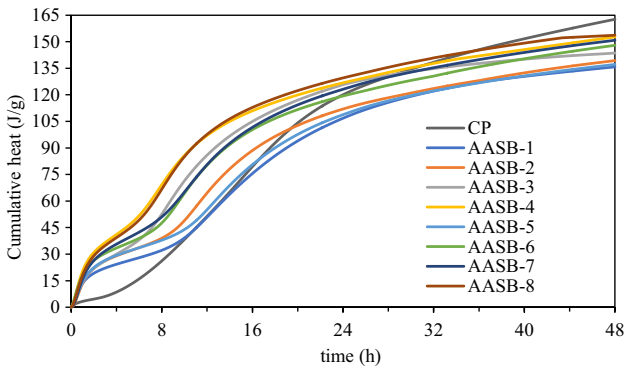

Fig. 9 Cumulative heat rate of a CP and all the AASB samples

process in AASBs and highlights the need to consider multiple parameters for a comprehensive understanding of their heat release behaviour.

3.4 XRD

Figure 11 displays the distinctive X-ray diffraction (XRD) patterns for a cement sample and eight samples of alkali-activated slag bider (AASB) at the 28-day mark. In the AASB's results, noticeable broad peaks with varying intensities are observed, which is a result of both the unreacted slag and the amorphous reaction products. Identification of the reaction products in the AASB samples was achieved by comparing the measured peaks with the literature values 2θ (Reddy and Subramaniam 2020).

The XRD patterns reveal prominent diffraction peaks at approximately 29.5 degrees 2-theta (2θ), while a less distinct reflection around 50 degrees 2θ is associated with the presence of C–A–S–H gel (Ben Haha et al. 2011; Liu et al. 2018). Additionally, less defined peaks at approximately 32 degrees and 40 degrees 2θ, which are identifiable in certain AASB samples, are identified as Gehlenite and hydrotalcite,

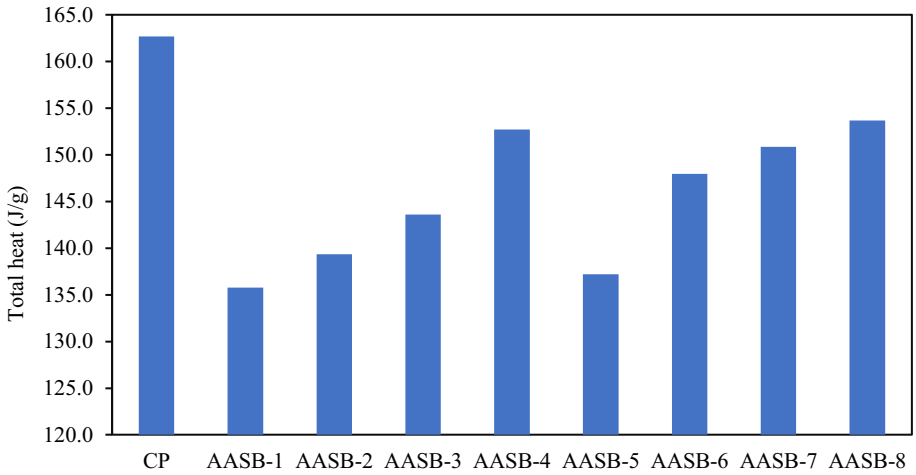

Fig. 10 Total heat in 48 h of hydration heat testing for a CP and all AASB samples

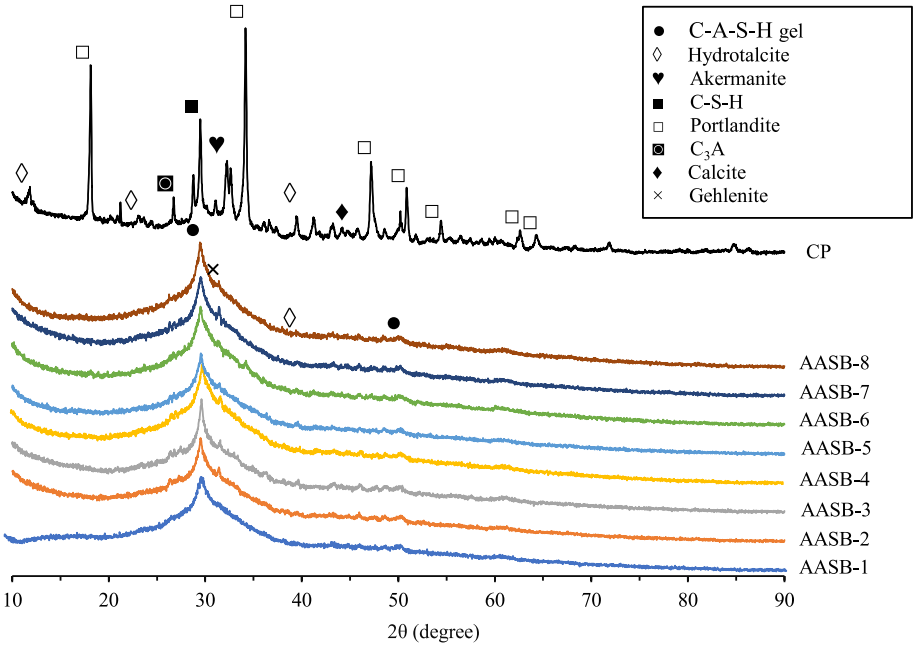

Fig. 11 XRD analysis of CP and AASB samples at the age of 28 days

respectively (Reddy and Subramaniam 2020). The C–A–S–H phase at 29.5 degrees 2θ and 50 degrees 2θ indicates that the hydration products formed in sodium hydroxide and sodium silicate-activated slag are more amorphous compared to those in the cement sample. Moreover, indistinct peaks at 32 degrees and 40 degrees 2θ, corresponding to Gehlenite and hydrotalcite-like phases, are not consistently detected in some AASB samples, potentially due to non-uniform sampling, as confirmed by subsequent FE-SEM analysis. Significantly, a broad diffraction peak spanning from 22° to 38° 2θ is evident in the AASB curves, signifying the development of an amorphous three-dimensional network structure, aligning with the outcomes of the FE-SEM analysis. The XRD analysis indicates that the intensity of hydration products, including C–A–S–H gel, Gehlenite, and hydrotalcite, varies with the concentration of Na_2O percentage and the activator modulus used (Almakhadmeh and Soliman 2021). Notably, the intensity of the hydration products, including C–A–S–H phase, increases with higher concentrations of the activator solution. The AASB-8 sample, featuring a Na_2O percentage of 7% and an activation modulus of 1.2, exhibits a more pronounced intensity peak of the C–A–S–H phase compared to the samples with lower Na_2O percentages and activation modulus values.

3.5 Thermogravimetric Analysis (TGA)

Figure 12 illustrates the thermogravimetry (TG) and differential thermogravimetry (DTG) profiles of a cement sample alongside eight AASB samples. The results reveal that mixes AASB-4 and AASB-8 exhibited weight losses of 16.6% and 15.9%, respectively, in contrast to mixes CP, AASB-1,

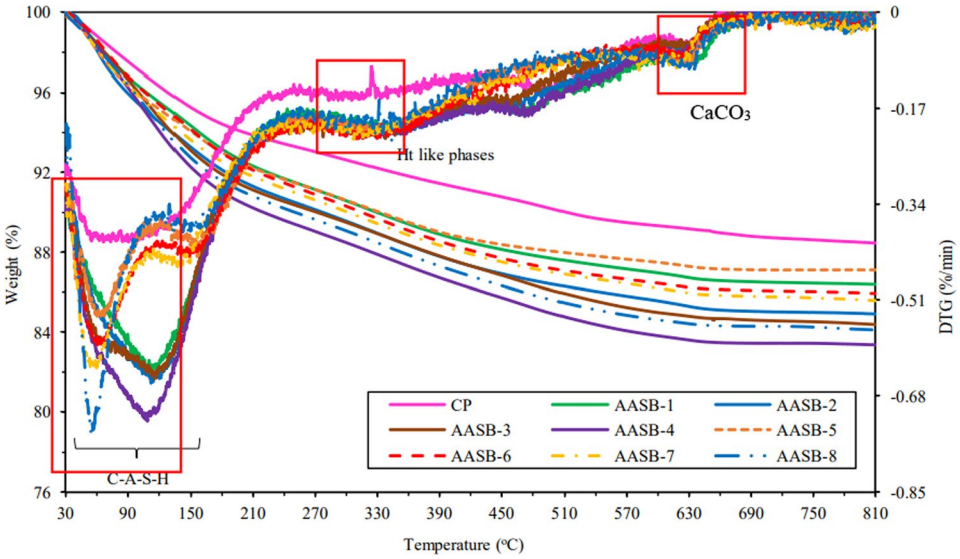

Fig. 12 TGA results of a CP and eight AASB samples at 28 days of curing

AASB-2, AASB-3, AASB-5, AASB-6, and AASB-7, which experienced losses of 11.5%, 13.6%, 15.1%, 15.6%, 12.9%, 14.1%, and 14.4%, respectively. Compared to the alkaline binders, cement paste displayed a lower degree of hydration in initial phases. The observed trend indicates a positive correlation, suggesting that an increase in activator concentration leads to enhanced hydration levels and the synthesis of diverse products. Elevating the Na_2O activator dosage resulted in a higher concentration of hydroxide species in the aqueous phase and accelerating the rate of precursor dissolution. This increase in dissolved species, including silicon (Si) and aluminium (Al), facilitated the formation of various phases of hydration products. The higher silica modulus preference for Si species and increased Si bridging accommodated dissolved species, forming a more intricate compound structure, such as calcium–aluminium–silicate-hydrate (C–A–S–H). AASB pastes exhibited significantly greater mass reduction than CP at the same age, indicating a higher amount of hydration products, consistent with hydration heat findings.

The inferior performance of pure cement after exposure to high temperatures may be attributed to changes in chemical structure and product dehydration. AASB demonstrated exceptional fire resistance, with a substantial mass reduction occurring below 800 °C, indicating minimal decomposition of hydration products beyond this threshold. In the temperature range of 50 to 70 °C, characteristic peaks were observed, linked to dehydration or decomposition of calcium aluminosilicate hydrate (C–A–S–H) gel and free water that may have been absorbed during sample preparation (Angulo-Ramírez et al. 2017). Additional small peaks between 300 and 400 °C were likely due to the dehydration of hydrotalcite (Ben Haha et al. 2011; Ismail et al. 2013; Zheng and Zhu 2013). Slag-activated with a higher concentration of alkali activator exhibited increased weight loss, aligning with the X-ray diffraction results. Cement paste (CP) samples exposed to high temperatures generally undergo three decomposition reactions: dehydration of C–S–H gel in the temperature range of 100–150 °C, decomposition of hydrated calcium hydroxide ($Ca(OH)_2$) occurring around 350–450°C, and decarbonisation of $CaCO_3$ resulting from the carbonation reaction of calcium hydroxide at roughly 600–700°C (Salman et al. 2015a). In the AASB system, $Ca(OH)_2$ and $CaCO_3$ decomposed at lower temperatures, possibly due to the presence of alkali promoting carbonate phase decomposition. Another possible explanation is that the formed carbonates are partly amorphous, which causes poorly crystallized $Ca(OH)_2$ and $CaCO_3$ to decompose at lower temperatures (Salman et al. 2015b; Sun and Chen 2019).

3.6 FE-SEM/EDX

In this section, the micro-structure of AASB is examined using a field emission scanning electron microscope (FE-SEM), focusing on the influence of Na_2O percentage and activator modulus on the outcomes. Figure 13a presents the FE-SEM image of CP, while Fig. 12b–i showcases FE-SEM images of AASB prepared with Na_2O concentration of 4–7% and an activator modulus of 1.2 and 1.0. When GGBS is activated by an alkaline solution, it results in the formation of a C–A–S–H gel. The results affirm that the primary hydration product of AAS is the gel-like phase of calcium-silicate-hydrate, after combined with aluminium to produce a calcium aluminosilicate hydrate (C–A–S–H) gel (Los, n.d.). Notably, enough C–A–S–H gel was produced, effectively filling pores, and compacting the matrix. However, some micro-cracks and residual slag particles were identified.

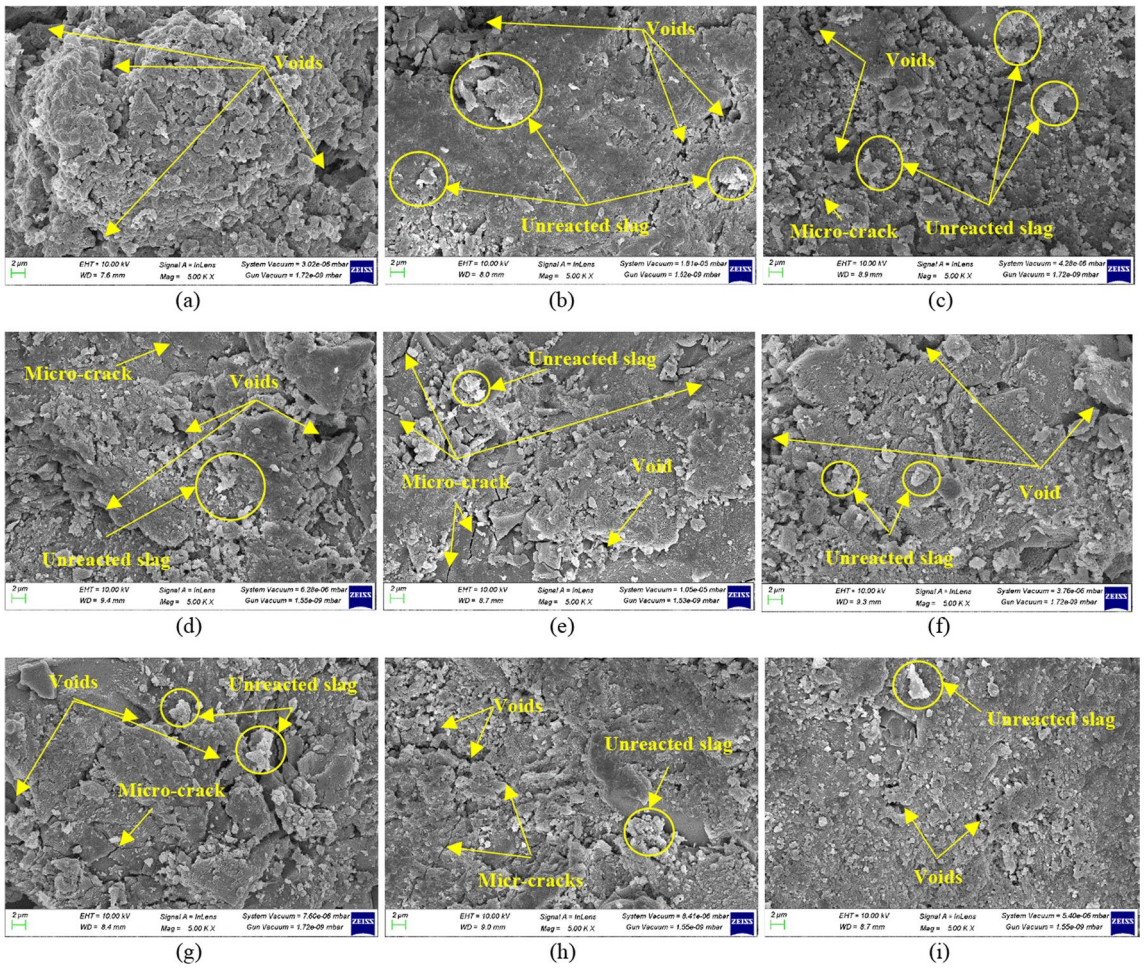

Fig. 13 FE-SEM results of **a** CP, **b** AASB-1, **c** AASB-2, **d** AASB-3, **e** AASB-4, **f** AASB-5, **g** AASB-6, **h** AASB-7, and **i** AASB-8

The FE-SEM image of AASB-8 reveals a denser and more uniform matrix with fewer voids compared to CP and other AAS binders, consistent with compressive test results. Nevertheless, micro-cracks are still visible, as depicted in Fig. 13i. Some of the cracks appearing may have been created while preparing the samples for FE-SEM analysis. Similar findings were observed in the micro-structure of AASB-4. Figure 13 indicates that samples with higher concentration of alkaline solution exhibit more cracks due to their brittle structure. This brittleness may result from the adverse impact of OH^- ions on the activation process (Ruiz-Santaquiteria et al. 2012). Additionally, increasing the Na_2O percentage in the alkaline solution resulted in an increase of Na atoms' concentration, which could lead to the brittleness upon integration into the C–A–S–H gel framework. Other researchers' findings support these observations, indicating that increasing Na_2O concentration and silicate content in an alkali activator solution for GGBS-based systems can refine the pores and densify the micro-structure (Cihangir et al. 2015; Jafari Nadoushan and Ramezanianpour 2016; Phoo-Ngernkham et al. 2015). AASB samples with lower alkaline solution concentration exhibits a looser micro-structure due to poor hydration. The randomly embedded C–A–S–H gel in AAS samples aligns with XRD findings. Furthermore, the micro-structure of some AASB samples is denser than CP. The denser micro-structure of AASB is due to the pozzolanic effect of slag, which consumes a significant amount of $Ca(OH)_2$ with a coarse crystal structure and enhances the interface orientation. Despite the denser micro-structure, unreacted slag is visible, possibly contributing to the lower compressive strength of the alkali-activated slag binder.

Energy-dispersive X-ray spectroscopy (EDX) analysis was conducted for each sample and results presented in Table 7. The analysis indicates different reaction products for each sample, with Ca/Si and Al/Si ratios suggesting the presence of calcium silicate hydrate and aluminosilicate hydrate phases. These observations align with previous studies noting the coexistence of a geo-polymeric gel and

Table 7 Details of the atomic percentage of elements shown in EDX plots

Sample	Atomic %									
	C	O	Na	Mg	Al	Si	Ca	Ca/Si ratio	Al/Si ratio	Na/Si ratio
CP	19.01	43.29	0.05	0.63	1.47	0.73	28.88	39.56	2.01	0.07
AASB-1	29.5	40.94	4.46	2.22	4.65	8.27	8.98	1.09	0.56	0.54
AASB-2	13.58	46.44	6.14	1.56	5.24	12.43	12.75	1.03	0.42	0.49
AASB-3	25	43.59	6.4	1.42	4.44	8.65	10.52	1.22	0.51	0.74
AASB-4	15.15	49.91	7.55	1.99	5.21	10.71	7.78	0.73	0.49	0.70
AASB-5	10.51	37.03	9.06	2.41	5.83	14.85	13.55	0.91	0.39	0.61
AASB-6	24.35	45.31	5.57	1.02	5.28	8.86	8.43	0.95	0.60	0.63
AASB-7	19.94	44.74	6.35	1.63	5.31	10.93	10.48	0.96	0.49	0.58
AASB-8	20	45.77	4.25	1.28	3.14	8	15.77	1.97	0.39	0.53

calcium silicate hydrate gel within a single binder (Reddy and Subramaniam 2020; Shariati et al. 2021).

4 Conclusions

This study investigated the use of two different activators, NaOH and sodium silicate, along with eight varying concentrations of the alkaline solution to generate eight distinct AAS binders and mortars. Calorimetric studies were carried out to analyse the early-stage hydration processes in the AAS binders in comparison with cement paste (CP). Furthermore, the study aimed to evaluate the physical and mechanical properties of alkali-activated slag mortar (AASM), with a specific focus on its compressive strength. Advanced techniques, including X-ray diffraction (XRD), field emission scanning electron microscopy (FE-SEM), thermogravimetry analysis (TGA), and energy-dispersive X-ray spectroscopy (EDX), were employed to understand the reaction mechanism and products of alkali-activated slag binder. The results of the study can be summarized as follows:

- AAS binders typically exhibit higher compressive strength and the formation of a denser and more stable micro-structure compared to ordinary Portland cement paste (CP), especially at early ages. This superiority to the increased amount of amorphous calcium silicate hydrate (C–A–S–H) gel formed during the slag and alkali activator reaction.
- The study indicates that increasing the Na_2O concentration from 4 to 7% and the activation modulus from 1.0 to 1.2, with a constant water/binder ratio of 0.40, positively impacts the compressive strengths of AAS mortars.
- X-ray diffraction (XRD) analysis highlights an amorphous phase in the geo-polymerization reaction of AAS binders, contrasting with the dual-phase nature (amorphous and crystalline) of the control paste of OPC.
- The study implies that AAS binders with a Na_2O percentage equal to or below 4% may contain unreacted slag particles, potentially affecting mechanical properties and long-term durability. It is recommends considering these particles in the design of AAS-based materials for optimal performance over an extended period.
- Optimizing the mixture composition results in the formation of C–A–S–H gel, the compressive strength of AASM-4 mix mortar cubes under room temperature curing reaches 89.4 MPa after 28 days, deemed satisfactory for concrete with favourable mechanical properties. This strength is achieved with a Na_2O concentration of 7% and an activation modulus of 1.2 while maintaining a water-to-binder ratio of 0.40. Furthermore, mortar cubes featuring Na_2O concentration between 4 to 7% were found to achieve over 70% of their 28-day compressive strength within a period of 7 days.
- The study finds comparable hydration mechanisms between alkali-activated steel slag and cement. The alkali-activated slag binder exhibits a shorter dormant stage, an earlier and higher second exothermic peak, and lower cumulative heat in the first 48 h compared to cement. A positive correlation between calorimetric peak and compressive strength development is noted. Based on the findings, it can be concluded that alkali-activated slag binders should not be considered as low-heat cement/binder.
- FE-SEM and TGA results indicate that the primary product of AAS binder hydration is C–A–S–H. Higher alkaline activator concentration results in denser, more uniform morphology with fewer pores, emphasizing the crucial role of activator concentration in determining AAS binder paste morphology and porosity.
- The pore structure of hardened AAS binder pastes activated by sodium silicate and sodium hydroxide is more compact than that of cement paste. Alkali-activated slag (AAS) mortar exhibits a 52–89% increase compressive strength compared to cement mortar suggesting the potential of AAS binder to replace cement in specific engineering applications requiring high strength.

- Furthermore, AAS binder, produced in room temperature curing conditions, demonstrates a low embodied energy profile, utilizes industrial by-products, and generates significantly lower CO_2 emissions than ordinary Portland cement. Given its comparable or superior characteristics and effectiveness, AAS binder may be considered a sustainable substitute for Portland cement.

Acknowledgements The support from my supervisors, Professor Pramod Kumar Gupta and Professor Mohd. Ashraf Iqbal from the Department of Civil Engineering, Indian Institute of Technology Roorkee, India, is gratefully acknowledged.

Author Contributions SK was involved in the conceptualization, methodology, investigation, resources, writing—original draft. PKG contributed to reviewing and editing, supervision, project administration, funding acquisition, and review and editing. MAI assisted in the supervision and project administration.

Declarations

Conflict of interest The authors declare that they have no known competing financial interests or personal relationships that could have appeared to influence the work reported in this paper. The authors declare that the manuscript is the author's original work and has not been published before.

References

Al Makhadmeh W, Soliman A (2020) Effect of activator nature on property development of alkali-activated slag binders. J Sustain Cem Mater 10:240–256. https://doi.org/10.1080/21650373.2020.1833256

Al Makhadmeh W, Soliman A (2022) On the mechanisms of shrinkage reducing admixture in alkali activated slag binders. J Build Eng 56:104812. https://doi.org/10.1016/j.jobe.2022.104812

Almakhadmeh M, Soliman AM (2021) Effects of mixing water temperatures on properties of one-part alkali-activated slag paste. Constr Build Mater 266:121030. https://doi.org/10.1016/j.conbuildmat.2020.121030

Angulo-Ramírez DE, Mejía de Gutiérrez R, Puertas F (2017) Alkali-activated Portland blast-furnace slag cement: mechanical properties and hydration. Constr Build Mater 140:119–128. https://doi.org/10.1016/j.conbuildmat.2017.02.092

Arioz E, Arioz O, Kockar OM (2020) Geopolymer synthesis with low sodium hydroxide concentration. Iran J Sci Technol Trans Civ Eng 44:525–533. https://doi.org/10.1007/s40996-019-00336-1

Ben Haha M, Le Saout G, Winnefeld F, Lothenbach B (2011) Influence of activator type on hydration kinetics, hydrate assemblage and microstructural development of alkali activated blast-furnace slags. Cem Concr Res 41:301–310. https://doi.org/10.1016/j.cemconres.2010.11.016

Bilim C, Karahan O, Atiş CD, İlkentapar S (2015) Effects of chemical admixtures and curing conditions on some properties of alkali-activated cementless slag mixtures. KSCE J Civ Eng 19:733–741. https://doi.org/10.1007/s12205-015-0629-0

Bingöl Ş, Bilim C, Atiş CD, Durak U (2020) Durability properties of geopolymer mortars containing slag. Iran J Sci Technol Trans Civ Eng 44:561–569. https://doi.org/10.1007/s40996-019-00337-0

Brough AR, Atkinson A (2002) Sodium silicate-based, alkali-activated slag mortars—part I. Strength, hydration and microstructure. Cem Concr Res 32:865–879. https://doi.org/10.1016/S0008-8846(02)00717-2

Cao R, Zhang S, Banthia N, Zhang Y, Zhang Z (2020) Interpreting the early-age reaction process of alkali-activated slag by using combined embedded ultrasonic measurement, thermal analysis, XRD, FTIR and SEM. Compos Part B Eng 186:107840. https://doi.org/10.1016/j.compositesb.2020.107840

Cihangir F, Ercikdi B, Kesimal A, Deveci H, Erdemir F (2015) Paste backfill of high-sulphide mill tailings using alkali-activated blast furnace slag: effect of activator nature, concentration and slag properties. Miner Eng 83:117–127. https://doi.org/10.1016/j.mineng.2015.08.022

IS: 4031 (Part 6) (2006) Determination of compressive strength of hydraulic cement other than masonry cement. Bur Indian Stand Delhi 1–11

Humad AM, Habermehl-Cwirzen K, Cwirzen A (2019) Effects of fineness and chemical composition of blast furnace slag on properties of alkali-activated binder. Materials (basel) 12:1–16. https://doi.org/10.3390/ma12203447

IS 650:1991 (1991) Indian specification for standard sand for testing of cement. Indian Stand. 1–11

Ismail I, Bernal SA, Provis JL, Hamdan S, Van Deventer JSJ (2013) Drying-induced changes in the structure of alkali-activated pastes. J Mater Sci 48:3566–3577. https://doi.org/10.1007/s10853-013-7152-9

Jafari Nadoushan M, Ramezanianpour AA (2016) The effect of type and concentration of activators on flowability and compressive strength of natural pozzolan and slag-based geopolymers. Constr Build Mater 111:337–347. https://doi.org/10.1016/j.conbuildmat.2016.02.086

Kar A, Ray I, Halabe UB, Unnikrishnan A, Dawson-Andoh B (2014) Characterizations and quantitative estimation of alkali-activated binder paste from microstructures. Int J Concr Struct Mater 8:213–228. https://doi.org/10.1007/s40069-014-0069-0

Kumar S, Gupta PK, Iqbal MA (2023a) Parametric sensitivity analysis of high-strength self-compacting alkali-activated slag concrete for enhanced microstructural and mechanical performance. Iran J Sci Technol Trans Civ Eng. https://doi.org/10.1007/s40996-023-01227-2

Kumar S, Kumar Gupta P, Ashraf Iqbal M (2023b) An experimental study on the development of self-compacting alkali-activated slag concrete mixes under ambient curing. Today Proc, Mater. https://doi.org/10.1016/j.matpr.2023.03.558

Lanjewar BA, Chippagiri R, Dakwale VA, Ralegaonkar RV (2023) Application of alkali-activated sustainable materials: a step towards net zero binder. Energies. https://doi.org/10.3390/en16020969

Liu S, Li Q, Han W (2018) Effect of various alkalis on hydration properties of alkali-activated slag cements. J Therm Anal Calorim 131:3093–3104. https://doi.org/10.1007/s10973-017-6789-z

Los, U.M.D.E.C.D.E., n.d. No 主観的健康感を中心とした在宅高齢者における 健康関連指標に関する共分散構造分析Title.

Mangat PS, Ojedokun OO, Lambert P (2021) Chloride-initiated corrosion in alkali activated reinforced concrete. Cem Concr Compos 115:103823. https://doi.org/10.1016/j.cemconcomp.2020.103823

Mareya M, Bahurudeen A, Varghese J, Thomas BS, Sithole NT (2023) Transformation of rice husk modified basic oxygen furnace slag into geopolymer composites. J Mater Res Technol 24:6264–6278. https://doi.org/10.1016/j.jmrt.2023.04.225

Nasr D, Pakshir AH, Ghayour H (2018) The influence of curing conditions and alkaline activator concentration on elevated temperature behavior of alkali activated slag (AAS) mortars. Constr Build Mater 190:108–119. https://doi.org/10.1016/j.conbuildmat.2018.09.099

Navarro R, Zornoza E, Sánchez I, Alcocel EG (2022) Influence of the type and concentration of the activator on the microstructure of

alkali activated SiMn slag pastes. Constr Build Mater. https://doi.org/10.1016/j.conbuildmat.2022.128067
Pandhare SJ, Jayaraj DMGK (2023) Properties of high volume ggbfs and high volume flyash concrete: a brief review. Int J Res Appl Sci Eng Technol 11:491–494. https://doi.org/10.22214/ijraset.2023.49435
Phoo-Ngernkham T, Maegawa A, Mishima N, Hatanaka S, Chindaprasirt P (2015) Effects of sodium hydroxide and sodium silicate solutions on compressive and shear bond strengths of FA-GBFS geopolymer. Constr Build Mater 91:1–8. https://doi.org/10.1016/j.conbuildmat.2015.05.001
Provis JL (2018) Alkali-activated materials. Cem Concr Res 114:40–48. https://doi.org/10.1016/j.cemconres.2017.02.009
Reddy KC, Subramaniam KVL (2020) Blast furnace slag hydration in an alkaline medium: influence of sodium content and sodium hydroxide molarity. J Mater Civ Eng 32:1–10. https://doi.org/10.1061/(asce)mt.1943-5533.0003455
Ruiz-Santaquiteria C, Skibsted J, Fernández-Jiménez A, Palomo A (2012) Alkaline solution/binder ratio as a determining factor in the alkaline activation of aluminosilicates. Cem Concr Res 42:1242–1251. https://doi.org/10.1016/j.cemconres.2012.05.019
Runci A, Serdar M (2022) Effect of curing time on the chloride diffusion of alkali-activated slag. Case Stud Constr Mater 16:e00927. https://doi.org/10.1016/j.cscm.2022.e00927
Runci A, Provis J, Serdar M (2022) Microstructure as a key parameter for understanding chloride ingress in alkali-activated mortars. Cem Concr Compos 134:104818. https://doi.org/10.1016/j.cemconcomp.2022.104818
Salman M, Cizer Ö, Pontikes Y, Snellings R, Dijkman J, Sels B, Vandewalle L, Blanpain B, Van Balen K (2015a) Alkali activation of AOD stainless steel slag under steam curing conditions. J Am Ceram Soc 98:3062–3074. https://doi.org/10.1111/jace.13776
Salman M, Cizer Ö, Pontikes Y, Snellings R, Vandewalle L, Blanpain B, Balen KV (2015b) Cementitious binders from activated stainless steel refining slag and the effect of alkali solutions. J Hazard Mater 286:211–219. https://doi.org/10.1016/j.jhazmat.2014.12.046
Schade T, Bellmann F, Middendorf B (2022) Quantitative analysis of C–(K)–A–S–H-amount and hydrotalcite phase content in finely ground highly alkali-activated slag/silica fume blended cementitious material. Cem Concr Res. https://doi.org/10.1016/j.cemconres.2021.106706
Shariati M, Shariati A, Trung NT, Shoaei P, Ameri F, Bahrami N, Zamanabadi SN (2021) Alkali-activated slag (AAS) paste: correlation between durability and microstructural characteristics. Constr Build Mater 267:120886. https://doi.org/10.1016/j.conbuildmat.2020.120886
Shi C, Day RL (1996) Some factors affecting early hydration of alkali-slag cements. Cem Concr Res 26:439–447. https://doi.org/10.1016/S0008-8846(96)85031-9
Shi C, Krivenko PV, Roy DM (2006) Alkali-activated cements and concretes. Taylor & Francis
Sithole NT, Mashifana T (2020) Geosynthesis of building and construction materials through alkaline activation of granulated blast furnace slag. Constr Build Mater 264:120712. https://doi.org/10.1016/j.conbuildmat.2020.120712
Sithole NT, Okonta F, Ntuli F (2019) Development of lightweight construction blocks by alkaline activation of bof slag. J Solid Waste Technol Manag 45:175–185. https://doi.org/10.5276/JSWTM/2019.175
Sithole T, Mashifana T, Tsotetsi N (2021a) Enhancement of waste foundry sand mechanical properties through stabilization using slag based geopolymer binder 1–25
Sithole T, Tsotetsi N, Mashifana T (2021b) Synthesis of ambient cured ggbfs based alkali activated binder using a sole alkaline activator: a feasibility study. Appl Sci. https://doi.org/10.3390/app11135887
Sithole NT, Tsotetsi NT, Mashifana T, Sillanpää M (2022) Alternative cleaner production of sustainable concrete from waste foundry sand and slag. J Clean Prod. https://doi.org/10.1016/j.jclepro.2022.130399
Sun J, Chen Z (2019) Effect of silicate modulus of water glass on the hydration of alkali-activated converter steel slag. J Therm Anal Calorim 138:47–56. https://doi.org/10.1007/s10973-019-08146-3
Tushar D, Das D, Pani A, Singh P (2022) Geo-engineering and microstructural properties of geopolymer concrete and motar: a review. Iran J Sci Technol Trans Civ Eng 46:2713–2737. https://doi.org/10.1007/s40996-021-00756-y
Usherov-marshak A, Vaičiukynienė D, Krivenko P, Bumanis G (2021) Calorimetric studies of alkali-activated blast-furnace slag cements at early hydration processes in the temperature range of 20–80 °C. Materials (basel). https://doi.org/10.3390/ma14195872
Venkatesan RP, Pazhani KC (2016) Strength and durability properties of geopolymer concrete made with ground granulated blast furnace slag and black rice husk ash. KSCE J Civ Eng 20:2384–2391. https://doi.org/10.1007/s12205-015-0564-0
Wang A, Zheng Y, Zhang Z, Liu K, Li Y, Shi L, Sun D (2020) The durability of alkali-activated materials in comparison with ordinary Portland cements and concretes: a review. Engineering 6:695–706. https://doi.org/10.1016/j.eng.2019.08.019
Zhang Y, Zhang S, Chen Y, Çopuroğlu O (2022) The effect of slag chemistry on the reactivity of synthetic and commercial slags. Constr Build Mater. https://doi.org/10.1016/j.conbuildmat.2022.127493
Zheng W, Zhu J (2013) The effect of elevated temperature on bond performance of alkali-activated GGBFS paste. J Wuhan Univ Technol Mater Sci Ed 28:721–725. https://doi.org/10.1007/s11595-013-0759-5